O'Sullivan-Greene, E., T. Kameneva, D. Trevaks, A. Shafton, S. C. Payne, R. McAllen, J. B. Furness, and D. B. Grayden. 2018. Modeling experimental recordings of vagal afferent signaling of intestinal inflammation for neuromodulation. *Journal of Neural Engineering*. **15**(5): 056032.

doi: 10.1088/1741-2552/aad96d

Modeling experimental recordings of vagal afferent signaling of intestinal inflammation for neuromodulation applications

Elma O'Sullivan-Greene[1,^], Tatiana Kameneva,[1,2,^*], David Trevaks[3], Anthony Shafton[3], Sophie C. Payne[4], Robin McAllen[3,4], John B. Furness[3,5], David B. Grayden[1,]*

*[1] Department of Biomedical Engineering, The University of Melbourne, Australia; [2] Faculty of Science, Engineering and Technology, Swinburne University of Technology, Australia; [3] Florey Institute of Neuroscience and Mental Health, Australia; [4] Bionics Institute, Australia; [5] Department of Anatomy and Neuroscience, The University of Melbourne, Australia; * corresponding author: tkameneva@swin.edu.au*
[^]These authors contributed equally to this work.

Abstract

Objective
Artificial modulation of peripheral nerve signals (neuromodulation) by electrical stimulation is an innovation with potential to develop treatments that replace or supplement drugs. One function of the nervous system that can be exploited by neuromodulation is regulation of disease intensity. Optimal interfacing of devices with the nervous system requires suitable models of peripheral nerve systems so that closed-loop control can be utilized for therapeutic benefit.
Approach
We use physiological data to model afferent signaling in the vagus nerve that carries information about inflammation in the small intestine to the brain.
Main results
The vagal nerve signaling system is distributed and complex; however, we propose a class of reductive models using a state-space formalism that can be tuned in a patient-specific manner.
Significance
These models provide excellent fits to a large range of nerve recording data but are computationally simple enough for feedback control in implantable neuromodulation devices.

INTRODUCTION

The neural circuitry that controls the gastrointestinal tract has been extensively studied in recent years, which has allowed neural circuit diagrams to be drawn up in considerable detail (Furness et al. 2014). In particular, it is known that the vagus nerves are the main afferent conduit for the transmission of information about the physiological state of the intestine to the brain. On the other hand, inflammatory tissues within the intestine are innervated and controlled from the central nervous system by sympathetic nerve pathways and the transmitters released from sympathetic nerves have anti-inflammatory effects (Lomax et al. 2010, Stemberg 1997, Willemze et al. 2015, Willemze et al. 2017).

Inflammatory Bowel Disease (IBD) is common, persists for many years, and is difficult to treat. It is often refractory to current treatments, which in some cases also cause undesired side effects. For these reasons, non-pharmaceutical approaches, notably neuromodulation, have been proposed for the treatment of this and other inflammatory conditions (Bonaz 2016). In recent years, the vagus nerve has been implicated as a key site for exerting anti-inflammatory effects, and its stimulation has been trialed in IBD with positive outcomes in a small group of patients (Bonaz et al. 2016). Vagal stimulation is thought to act in at least two ways: 1) stimulating efferent fibers to engage the 'cholinergic anti-inflammatory pathway' (Pavlov and

Tracey 2005); 2) stimulating vagal afferent fibers that normally inform the brain of the presence of peripheral inflammation and that engage anti-inflammatory sympathetic neural pathways back to tissues to reduce the intensity of inflammation (Martelli et al. 2014a, Marteli et al. 2014b, Sternberg 1997; Willemze et al. 2017). The relation of vagal afferent activity to sympathetic efferent activation has been little investigated, in particular responses of vagal afferents to intestinal inflammation have not been investigated. While it is true that IBD often involves the colon, about 45% of IBD is Crohn's Disease, which mostly affects the ileum, which was the target of our study. Crohn's Disease has a worse prognosis after surgery; it almost always re-occurs. Thus, the present study is directly relevant to a significant proportion of IBD occurrences.

Loss of integrity of the epithelial layer lining the gut wall is a key characteristic symptom of IBD (Gerova et al. 2011) and causes the gut to become leaky. The change in gut permeability during inflammation is detectable using electrodes that measure changes in the transmucosal impedance of the gut wall (Payne et al. 2018). There exist methods that allow *in vivo* measurements of changes in transmucosal impedance (Ivorra & Rubinsky 2007, Nicander et al. 1997, Peppenheiner & Volpp 1992).

There is potential to optimize neuromodulatory control when a closed-loop control system is used. Closed-loop neuromodulation systems have been used, for example, in people with paraplegia (Abbas and Chizeck 1991), in the management of medically refractory focal epilepsy and seizure control with high frequency electrical stimulation (Fountas et al. 2005, Nelson et al. 2011), in patients with Parkinson's disease (Rosin et al. 2011), and in patients with paralysis by stimulating spinal cord to restore hand function (Zimmermann and Jackson 2014). Neuromodulatory control via a closed-loop control system has many advantages, including the ability to optimize parameters online based on patient-specific data, thus improving efficacy, saving device power consumption, and, possibly, selectively activating targeted neural populations (Tukhlina and Rosenblum 2008; Gorzelic et al. 2013). Due to the episodic nature of IBD, therapy is often administered to patients longer than is clinically required. Closed-loop neuromodulation system can be activated only when required, thereby providing optimal patient-specific therapy.

Closed-loop feedback can be designed based on model-free or model-based frameworks. Model-free frameworks treat the physical system as a black box; model-based controllers require that the physical system is approximated using mathematical models. Models suitable for controller design need to tractable and simple enough with minimal required computation time and adaptable to different neuronal populations and different patients. One such model is the state-space framework, which describes a physical system as a set of input, output, and state variables by first-order differential equations (or difference equations for a discrete system).

In this work, we recorded afferent vagal activity in response to inflammation of the intestine and model this activity using a state-space framework. We fitted model parameters to individual experiments and analyzed model performance. We have used this knowledge of the circuitry to guide the physiological recordings and to devise a circuit on which to base the modeling.

METHODS

Experiments

All animal experiments were performed in accordance with guidelines of the National Health and Medical Research Council of Australia and were approved by the Animal Experimentation Ethics Committee of the

Florey Institute of Neuroscience and Mental Health. All animal experiments were approved by United States Army Medical Research and Material Command Animal Care and Use Review Office (ACURO).

Experiments were conducted on adult male Sprague-Dawley rats in the weight range, 300-450 g. Rats (n=20) were anesthetized with pentobarbital (60 mg/kg i.p) and a tracheal cannula inserted, through which anesthesia was maintained thereafter with isoflurane (2% in oxygen) delivered by artificial ventilation. The femoral artery and vein was cannulated. The abdomen was opened by a longitudinal incision. A 10 cm loop of small intestine was selected and exteriorized. Loose silk ligatures were tied around either end of the selected segment, sufficient to close the lumen but not damage the gut wall, in order to restrict the spread of the injected inflammatory agent. A plastic cannula to deliver the agent was inserted into the gut segment lumen and tied in place. In other cases, the segment was selectively denervated by carefully stripping all nerve fibers from the mesenteric blood vessels supplying it (Furness et al. 1995). The segment was then returned to the abdomen.

A silk suture was inserted into the stomach close to the esophageal junction, and retracted caudally to expose the anterior abdominal vagus nerve as it travelled along the esophagus. Overlying connective tissues were removed and spleen and liver lobes were freed and held back by gauze packs. The hepatic branch was identified at its junction with the anterior vagus, and prepared for dissection and recording. To expose the celiac branch, a silk suture in the caudal esophageal wall was retracted to rotate the caudal esophagus and expose the posterior vagus. The celiac branch was identified at its junction with the posterior vagus, and prepared for dissection and recording. Either the celiac or hepatic branch was prepared for recording under a pool of liquid paraffin, made watertight by lining the area with cotton wool swabs soaked in 4% agar. Nerves were placed over a small black Perspex platform and dissected with the help of a dissecting microscope. Thin afferent filaments (attached distally) were peeled from the nerve and lifted onto one of two fine silver wires. A strand of local connective tissue was lifted onto a second silver wire, and the nerve activity signal was recorded differentially between the two wires with a high input impedance preamplifier (Neurolog, Welwyn Garden City, U.K.), amplified, and filtered (gain 10K, bandpass 80-700 Hz) before being recorded to a computer (CED 1401 Plus interface and SPIKE2 software, Cambridge Electronic Design, Cambridge, U.K.).

The inflammatory agent, 2,4,6-trinitrobenzene sulphonic acid (TNBS), 0.1% in 1 ml of 30% ethanol, was injected into the lumen of the gut segment either through a cannula or directly with a fine hypodermic needle under visual control. After 5 minutes, the loose ligatures at each end of the segment were removed. Afferent multi-unit spike activity was recorded from the hepatic or celiac vagal nerve branches for at least 20 mins before and 1 hour after TNBS injection.

Transmucosal Impedance Measurements

Transmucosal impedance measurements were obtained simultaneously with neural recording in three animals. To achieve this, a multi-electrode array was placed within the lumen of the intestine. The electrode array comprised four platinum ring electrodes (3.2 mm^2 surface area) equally spaced along a 10 cm lead-wire assembly. Electrodes were approximately 1.2 mm in diameter. In one animal, Electrode E1 acted as a control and was not placed in the region of gut exposed to the inflammatory solution. Electrodes E2 – E4 were placed distal to E1 in a segment of gut that was isolated and exposed to the inflammatory solution for a total duration of 3 hours. In the other two animals, all four electrodes were placed in the region of gut exposed to the inflammatory solution.

Transmucosal impedance between intraluminal electrodes and a subcutaneous return was determined by measuring the peak voltage at the end of the first phase of a biphasic stimulus (25 µs/phase, 8 µs interphase gap) delivered between an active electrode and a remote return electrode. The current used to generate a peak voltage was 931 µA. The V_{total} value was then used to calculate total impedance (Z_{total}) using Ohm's law (Z = voltage/current). Following each acute experiment, the electrodes were explanted, cleaned, and re-tested in saline. There was no significant difference between pre- and post-experiment *in vitro* measures (paired t-test; $p \geq 0.05$).

Mathematical Modeling

Modeling efforts focused on development and fitting of a state-space model of the vagal afferent systems that responded to inflammation in the small intestine. A schematic diagram of afferent and efferent pathways used as a basis for modeling is illustrated in Fig. 1. The open-loop system was used in simulations. In Figure 1, only neural connections shown in green were used in modeling.

State-Space Model

We defined an inflammation index using the experimental transmucosal impedance measurements, Z, as an indicator for the degree of inflammation, or gut leakiness. A linear piece-wise function was used to interpolate data between measured points. The inflammation index, r, was calculated as the fractional change in inverse impedance (admittance), from the baseline level of $1/Z_0$ prior to TNBS application,

$$r = \left(\frac{\frac{1}{Z} - \frac{1}{Z_0}}{\frac{1}{Z_0}} \right).$$

Additionally, we defined a normalized inflammation index, r_n, that was calculated as the change in inverse impedance, from the baseline level of $1/Z_0$ prior to TNBS application, normalized by the maximum measured change in inverse impedance,

$$r_n = \left(\frac{\frac{1}{Z} - \frac{1}{Z_0}}{\frac{1}{Z_{\max}} - \frac{1}{Z_0}} \right).$$

The afferent response to inflammation was modelled as a state-space model, as illustrated in Fig. 2. We assume that two separate and independent neural populations with distinctive individual responses to difference input triggers can be used to model the data. Therefore, we set matrices **A** and **B** to be diagonal. We directly label the parameters corresponding to gut leakiness due to the inflammatory response in the gut from TNBS with subscript L (for leakiness) and the parameters associated with the initial insult of TNBS application with subecript I (for insult). The state-space model used in simulations is

$$\begin{bmatrix} x_I(t+1) \\ x_L(t+1) \end{bmatrix} = \underbrace{\begin{bmatrix} a_I & 0 \\ 0 & a_L \end{bmatrix}}_{\mathbf{A}} \begin{bmatrix} x_I(t) \\ x_L(t) \end{bmatrix} + \underbrace{\begin{bmatrix} b_I & 0 \\ 0 & b_L \end{bmatrix}}_{\mathbf{B}} \begin{bmatrix} u_I(t) \\ u_L(t) \end{bmatrix}$$
$$y(t) = \overbrace{\begin{bmatrix} c_I & c_L \end{bmatrix}}^{\mathbf{C}} \begin{bmatrix} x_I(t) \\ x_L(t) \end{bmatrix}. \quad (1)$$

the state variables, x, evolve over time as a weighted linear sum of the previous state and input terms, u. The output of the system, y, is the change in spike count from the baseline spike count level established prior to application of TNBS. The index, k, samples time. The matrix, **A,** captures the history dependence of the previous spike count on the current spike count. The matrix, **B,** captures how each input signal influences

the behavior of the system. This model incorporates separate but interdependent neural populations that have distinctive individual responses that are then proportionally combined (via matrix **C**) in a neural recording.

The two inputs to the system are $u_1 = \delta(t)$, a Dirac delta function at the time of TNBS onset representing the physical insult applied to the gut, and $u_2 = r(t)$ or $u_2 = r_n(t)$, the inflammation index that indicates the level of gut leakiness above baseline level due to TNBS-induced inflammation. The input, u_1, represents the time of the injection of TNBS, which is on a much shorter time scale than the duration of the recording; therefore, it is modelled as a discrete Dirac delta function. The amplitude of this function is set to one in all simulations.

An average inflammation level across all experimental recordings, $\bar{r}$ or $\bar{r}_n$, was used as an input to the model of nerve activity where simultaneously recorded nerve activity and transmucosal impedance data were not available. Model performance was compared when normalized and non-normalized inflammation indices were used as an input to the model.

The model parameters, **A**, **B**, and **C**, were optimized such that the modeled spike count, y, matched the electrophysiological data from individual animal recordings. MATLAB (MathWorks, R2016a) function, *ssest*, was used to solve the state-space equations; *ssest* uses a prediction-error minimization algorithm to optimize for the parameters.

Model Fit to Data

To quantify the model performance, we used Normalized Root Mean Squared Error (NRMSE) expressed as a percentage, defined as

$$\text{Model Fit (\%)} = 100\left(1 - \frac{\|y_{\text{measured}} - y_{\text{model}}\|}{\|y_{\text{measured}} - \bar{y}_{\text{measured}}\|}\right) \quad (2)$$

where y_{measured} is the measured spike count, $\bar{y}_{\text{measured}}$ is its mean, y_{model} is the predicted spike count given by the model, and $\|.\|$ is the Euclidean norm (ℓ^2-norm) of a vector,

$$\|\boldsymbol{x}\| = \sqrt{\sum_{i=1}^{N} |x_i|^2} \quad \text{for } \boldsymbol{x} = [x_1, x_2, \cdots, x_N]. \quad (3)$$

A 0% model fit corresponds to a model that is no better at fitting the measured data than a straight line equal to the mean of the data.

Variance of each experimental recording was calculated using the following process:

(i) Normalize spike counts across experiments by dividing each spike count time series by the maximum spike count recorded during that experiment.

(ii) Find signal variance every 5 minutes,

$$\sigma_t^2 = \frac{1}{N}\sum_{t=i}^{t=i+5\text{min}} (x_t - \mu)^2, \quad (4)$$

where σ_t^2 denotes variance at time t, x_t denotes the spike count at time t, N is the number of samples in the 5 min epoch starting at $t = i$, and μ is the mean value of x_t in the 5 min epoch starting at $t = i$.

(iii) Calculate the mean of the variance across the recording,

$$\sigma_i^2 = \frac{1}{N_5}\sum_{t=0}^{T}\sigma_t^2, \quad (5)$$

where σ_i^2 is the variance of experiment i, T is the time at the end of the recording, and N_5 is the number of 5 min epochs across the recording. The window time of 5 min was used to calculate the variance over 10 samples of spike rate recordings.

(iv) Normalize the variance results across all experiments in the set,

$$\sigma_i^2 \xrightarrow[\text{norm}]{} \frac{\sigma_i^2}{\max\{\sigma_1^2,\sigma_2^2,\cdots,\sigma_M^2\}}. \quad (6)$$

Model Adjustments

Several model adjustments were made to give flexibility within the model to conform to the considerably varied spike count time series trajectories of the afferent dataset. These adjustments were as follows.

Adjustment of TNBS onset time

There was some uncertainty about the precise time when the application of TNBS impacted the afferent nerves. The TNBS onset times are recorded manually when it is injected and experimental variation in the speed and duration of TNBS injection was expected. To effectively capture the positive increase in spike in nerve activity that appeared in a subset of our afferent recordings at the time of TNBS, we allowed the model fitting to adjust the TNBS onset time. Our model algorithm selected the TNBS onset time that gave the best NRMSE fit within a ±2 sec window of the recorded TNBS onset time.

Impedance inputs allowed to be either normalized or raw measurements

The model has an input, u_L, related to gut leakiness due to inflammation, which is based on impedance measurements, $Z(t)$, and their inverse admittance, $Y(t) = 1/Z(t)$. We considered both normalized, $u_L(t) = \frac{Y(t)-Y(t_0)}{Y(t_0)}$, and non-normalized, $u_L(t) = Y(t)$, impedance-based inputs, where t_0 is the time of baseline gut leakiness (before application of TNBS).

Use of matched impedance

For the recordings (n=3) that had matched impedance data (impedance and neural activity were recorded from the same animal), we compared the ability of the model to fit experimental data when input to the model (i.e., degree of inflammation) was taken as an average of all experimental recording or as the impedance recorded simultaneously with spiking data from the same animal.

RESULTS

Experiments

Gut admittance and vagal activity were recorded in three animals and vagal afferent responses alone in a further 17. Measured gut admittance (inverse of transmucosal impedance), averaged across animals and recording electrodes, is illustrated in Fig. 3. Results illustrate that the gut admittance, an indication of the degree of inflammation used as the input to the state-space model, is increased after application of TNBS It is logical to expect that the impedance values were stable prior to the TNBS application taking effect. However, due to biological variability and noise during recordings, in some cases the recorded impedance

values were slightly higher 10 minutes before the application of TNBS (the time point "-10 min" in Fig. 3) than at the moment of TNBS injection (prior to the TNBS application taking effect). This fact and normalization by the maximum measured change in inverse impedance, sometimes resulted in negative values for the inflammation index for t<0 in Fig. 3.

We recorded direct afferent neural signals in the celiac branch of the vagus nerve in nine animals (Fig. 4A). The activity took the form of asynchronous ongoing spikes from multiple fibers. There was a rapid response of the afferent fibers in the celiac branch of the vagus, followed by a sustained increase in action potential firing, suggesting that these nerves reacted directly to TNBS injection and then to the subsequent inflammation. The celiac branch innervates the small intestine and a portion of the fibers were connected to the segment of intestine prepared for inflammatory treatment with TNBS. The inclusion of fibers from the salient region of intestine was confirmed in advance of TNBS administration by a transient increase in ongoing activity when that segment of gut was distended by inflation with saline. However, the nerve sample was diluted by, a variable proportion of afferent fibers connected to other regions of the gut. Usually, the direct afferent response to TNBS had two distinct phases (see Fig. 4A). Phase 1, seen prominently in some recordings, was an immediate response to the noxious insult as the afferent activity increased within seconds and peaked within 1-2 minutes before gradually subsiding. Phase 2 was a delayed response associated with inflammation. This response was variable, but generally built up slowly after a delay of 10-30 minutes.

We recorded afferent signals from the hepatic vagal branch in 11 animals (Fig. 4B). These recordings also showed ongoing asynchronous multi-unit spike activity. There was a slowly developing response of hepatic afferents, which is consistent with cytokines released from the inflamed intestine reaching the liver (through portal vessels) in sufficient quantity to activate hepatic vagal afferent nerve terminals. The activity began to build up 20-40 minutes after TNBS application to the gut, and remained elevated for as long as recordings continued. With one exception (see below), the phase 1 activity seen in the celiac branch did not occur in the hepatic branch. In eight of these recordings, the mesenteric nerves had been previously cut, such that the responses in hepatic afferents must have been indirectly mediated by a non-neural signal, presumably humoral factors (e.g. cytokines) released from the inflamed gut segment and carried in the portal circulation to the liver (Fig. 1). In three other rats, the mesenteric nerves were left intact. In one case, there was an immediate response to TNBS, which we attributed to afferent fibers from the gut joining the hepatic vagal branch (Horn & Friedman 2004). Neural signals have been recorded as ongoing action potentials in filaments of the hepatic branch of the vagus.

Our interpretation of the results is that the celiac branch carries afferent fibers that directly innervate the inflamed intestine. This is consistent with previous anatomical studies (see Fig 1). On the other hand, the hepatic afferents are indirectly activated when inflammatory mediators reach the liver in the blood coming from the inflamed region via the portal circulation.

Mathematical Modeling

In three animals, nerve spike data was recorded simultaneously with gut impedance (one celiac and two hepatic recordings). We expect that, for simultaneously recorded gut impedance and nerve activity (i.e. matched impedance), the model should faithfully map the changes in the gut permeability, as measured by impedance, to an afferent nerve spike count that corresponds well to that experimentally recorded.

The results show that for one hepatic and one celiac recording, as shown in Fig. 5A and B, respectively, the case with matched input impedances faithfully replicated the recorded spike counts and vastly exceeded

model performance where input was instead the average impedance of non-simultaneously recorded experiments.

In the third matched hepatic experiment, as shown in Fig. 5C, the matched and average inputs perform similarly. In this experiment, the number of recorded spikes was small. Moreover, the spike count exhibited minimal change from the baseline after TNBS was applied circa 850 seconds. Given these unusual attributes of this spike count time series, it is reasonable to conclude that it is not representative. By contrast, considering two other examples shown in subplots A and B, these data establish that validity of the state space model is contingent on a faithful input signal to quantify gut impedance. This strengthens the argument for model parameters that are optimized animal- or patient-specifically.

For all other nerve recordings presented below, where no impedance data was recorded, we used the average impedance as the model input. The average was composed of the three impedance recordings in animals where impedance was recorded simultaneously with neural spike data.

Representative examples of model fits to the data are shown in Fig. 6 for celiac and hepatic recordings. Normalized impedance measurements were used as inputs to the state-space models as neural recordings and impedance measurements were from different animals. Results indicate that the state-space model is a good fit to experimental data. For these examples, no adjustment for TNBS onset time was required since the model replicated experimental data well.

Because the actual time of arrival of TNBS at the intestinal mucosa could differ from the time marked by the experimenter as the beginning of infusion, we used the response to estimate a true time of exposure of the intestinal lining to TNBS (see Methods). The result of TNBS onset time adjustment caused a marked improvement in model fits, as shown in Fig. 7A. The time shifts from experiment timestamps of TNBS onset have a median value of 0 as shown in Fig. 7B. The time of input, u_1, is the time of the recorded TNBS injection. This was done annotated manually in a lab book and small inaccuracies are to be expected. Since the time of the recording may be slightly different to the actual time of the TNBS injection, the correct time may be obtained by shifting the time of the insult (actual injection time of TNBS) to a slightly earlier or later time point.

Table 1 illustrates the values of matrices **A**, **B**, and **C** for each of the recording shown in Fig. 7A. Since the matrices **A** and **B** are diagonal by definition, we list only the diagonal values. As can be seen from the table, the system is stable, with a_I and a_L being smaller than 1. The best fit values are listed in the table.

Table 1. *Values of matrices A, B, and C for each experiment. Only diagonal values are provided for A and B as the off-diagonals are set to 0.*

Experiment #	a_I	a_L	b_I	b_L	c_I	c_L
HepAffExp008	*0.98*	*0*	*443*	*747*	*0.03*	*0.97*
HepAffExp014	*0.99*	*0.22*	*801*	*7274*	*0.80*	*0.20*
HepAffExp029	*0*	*0.91*	*344*	*872*	*0.91*	*0.09*
HepAffDNExp028	*0.37*	*0*	*542*	*4613*	*-0.05*	*1.05*
HepAffDNExp032	*0.97*	*0*	*441*	*4530*	*0.19*	*0.81*
HepAffDNExp036	*0.87*	*0*	*158*	*117809*	*0.92*	*0.08*
HepAffDNExp038	*0.99*	*0*	*10569*	*1636*	*0.04*	*0.96*
HepAffDNExp039	*0.93*	*0.93*	*50*	*572*	*4.30*	*-3.30*
HepAffDNExp048	*0.99*	*0.38*	*378*	*30082*	*0.60*	*0.40*

HepAffDNExp052	*0.98*	*0.25*	*514*	*88964*	*0.97*	*0.03*
HepAffDNExp053	*0.89*	*0*	*4037*	*20906*	*0.17*	*0.83*
CelAffExp001	*0.67*	*0.13*	*1102*	*15391*	*0.71*	*0.29*
CelAffExp002	*0.93*	*0.23*	*1005*	*264800*	*0.92*	*0.08*
CelAffExp013	*0.01*	*0.01*	*-22*	*-201204*	*-2.56*	*1.56*
CelAffExp020	*0.99*	*0.56*	*223*	*9143*	*0.75*	*0.25*
CelAffExp027	*0.98*	*0.68*	*1433*	*4409*	*0.62*	*0.38*
CelAffExp029	*0.99*	*0.39*	*452*	*9286*	*0.78*	*0.22*
CelAffExp034	*0.98*	*0.79*	*275*	*76436*	*0.87*	*0.13*
CelAffExp062	*0*	*0.01*	*113*	*243000*	*0.68*	*0.32*
CelAffExp072	0.85	0	933	22055	0.26	0.74

The use of normalized or non-normalized impedance inputs had a small impact on model fits for most of the dataset. There were some experiments, however, where the state-space model found more optimal parameters in terms of model fit with either the normalized input or the non-normalized inputs, as shown in Fig. 8.

Fig. 9 shows a summary of the model performances for the different afferent experiments involving hepatic and celiac recordings. Because of the low-pass filtering used in the model, a fit of 80% is considered an excellent fit in this context. To assist in interpreting the performance measures, examples of the model fit percentages are shown in Fig. 10. Fig. 10A and B illustrate good and poor fits, respectively. Fig. 10C illustrates how the NRMSE goodness of model fit metric gives low fit values where the variance of the data is high.

Discussion

The electrophysiological recordings indicate that inflammation of the intestine evokes two phases of discharge in vagal afferent fibers innervating the gut, as revealed in recordings from the celiac branch of the vagus that innervates the intestine via the mesenteric nerves (Berthoud et al. 1991; Hillsley et al. 1998). The hepatic branch of the vagus innervates the liver, with a variable admixture of fibers joining from the intestine (Prechtl and Powley 1987; Phillips et al. 1997; Horn and Friedman 2004). However, the liver receives the venous drainage of the intestine via the portal vein and so tissue products, such as cytokines, that are released by inflammation will flow to the liver where they can activate afferents of the hepatic branch. Consistent with this, cytokines injected into the portal vein excite vagal afferents (Niijima 1996). In the present experiments, where the inflamed intestinal segment had been denervated, there was a slowly developing and sustained activation of nerve fibers in the hepatic branch of the vagus. These can only have arisen by a blood-borne route, as the neural route was ablated. In the case of the celiac branch, a rapid afferent fiber response was seen, consistent with there being a prominent direct neural response. Thus the two phases of discharge arise from the rapid activation of vagal afferents innervating the intestine by TNBS and a slower activation by inflammatory mediators that stimulate endings in the intestine, causing the delayed activity in the celiac branch, and enter the portal vein to cause the delayed response of hepatic afferents (see diagram of Fig. 1).

The information from multi-unit nerve recordings is semi-quantitative. This is because the population of activated fibers is diluted by an unknown proportion of fibers whose ongoing activity originates from regions not receiving the inflammatory stimulus. Nevertheless, the time profiles of responses are clear: 1) a

transient (~ 2 mins) direct response to the application of TNBS by fibers innervating the gut segment and coursing in the celiac vagal branch; 2) a delayed sustained response in both celiac and hepatic afferents that correlated with the build-up of inflammation and the breakdown of the mucosal barrier as measured by the fall in transmural impedance. We cannot quantitatively determine respective parts of activation of the hepatic versus the celiac vagus from our current data. Multiunit activity sampled from mixed nerves gives semi-quantitative information only. Both pathways send information about intestinal inflammation to the central nervous system. How the central nervous system responds to each of these signals is a subject of future investigation.

The results indicate that the brain receives both an integrated whole-of-gut signal and information about local inflammation and probably its intensity. The liver receives the venous drainage of the whole of the intra-abdominal gastrointestinal tract. Thus, wherever in the stomach, small and large intestine inflammatory mediators originate, they will impinge on the liver. The hepatic branch of the vagus will provide the central nervous system with information of the total inflammatory load experienced by the abdominal gastrointestinal tract. In addition, the central nervous system receives information about local inflammation through the celiac branch of the vagus. It remains to be determined how the central nervous system provides an appropriate response to the global and local inflammation. Detailed knowledge of the outputs from the central nervous system in response to different extents of gastrointestinal inflammation will illuminate this question.

Detailed understanding of the neuronal circuits involved in the control of enteric system is important for the development of optimal stimulation strategies in vagus nerve implants. For a review of vagus nerve stimulation to activate the anti-inflammatory pathways, see Bonaz et al. (2013) and Bonaz et al. (2016). The state of the art vagus nerve stimulation and recording strategies are discussed by Guiraud et al. (2016). A pilot study in patient with Crohn's disease (a chronic inflammatory disease of the intestines) indicated that vagus nerve stimulation may be an effective tool in the treatment of active Crohn's disease (Bonaz et al 2016). Abdominal vagus nerve stimulation in humans has been shown to prevent postoperative ileus and to reduce inflammation (Stakenborg et al. 2017). Vagus nerve stimulation has been also shown to attenuate the systemic inflammation in rats (Borovikova et al. 2000, Yamakawa et al 2013). Levine et al. (2014) showed that vagus nerve stimulation can activate the cholinergic anti-inflammatory pathway and significantly reduce activity in autoimmune disease model in rats.

The results indicate that a mathematical model of the enteric system could be used in closed-loop control to derive vagus nerve stimulation parameters online, using simultaneously recorded patient-specific data on the state of the intestine. Models of other aspects of the enteric system have also been proposed. Impulse-response function of splanchnic circulation with model-independent constraints has been proposed in (Munk et al. 2003). A model of enteric neural motor patterns is presented in (Chambers et al. 2014). Du et al. (2011) proposed a model of gastrointestinal electrochemical coupling that can be extended to relate electrical slow wave activity to motility in a multiscale framework. A role of fast and slow excitatory outputs of sensory neurons of the enteric neural circuits was explored using computer simulations in (Bornstein et al. 1997).

The class of state-space models proposed here is sufficiently adaptable and low (computational) complexity to be patient-specifically optimized in an implanted device environment. This adaptability may be advantageous in long term device trials to elucidate the mechanisms and actions of gut inflammatory response.

The quality of fits of the state-space models were markedly improved when simultaneous gut admittivity was measured with the neural recordings. This ensured that the input function to the model was more correctly represented. The gut admittivity over time was sufficiently similar between experiments that good fits could be obtained using the averaged time course. However, the improvement provided by the admittivity measurements suggests that it may be important to measure this in a future clinical device.

Conclusion

The models that we have developed enable us to investigate the intrinsic system information corresponding to gut leakiness in the inflamed intestine, while separating out the sampling-related artefacts that are specific to each experiment. These experiment-specific effects include the overall number of nerve fibers in the sample extracted for recording and the ratios of the various functional fiber types in the sampled subset. The study predicts the pattern of information that reaches the central nervous system, which may be used in the design of neuromodulation strategies to suppress gut inflammation through anti-inflammatory reflex pathways. Our analysis predicts that measures of gut leakiness could be used for closed-loop control of nerve stimulation for the suppression of intestinal inflammation.

Acknowledgements

This work was sponsored by the Defense Advanced Research Projects Agency (DARPA) BTO under the auspices of Dr. Doug Weber through the Space and Naval Warfare Systems Center Contract No. N66001-15-2-4060.

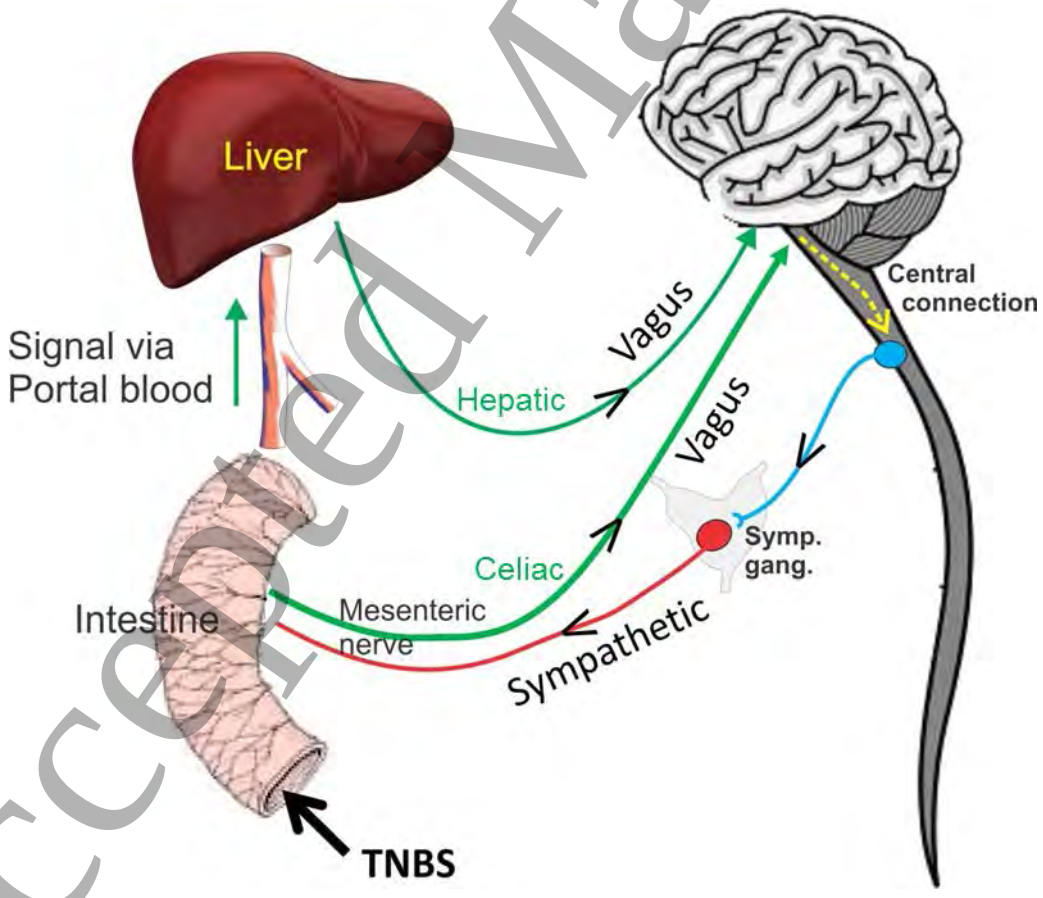

Figure 1. A schematic diagram of the relations between the intestine, liver, vagal afferents, and sympathetic efferents, showing the assumed physiological circuit for inflammatory signaling used for

modeling. When a region of intestine is inflamed, afferent signals are detected in the vagal nerve pathways that pass from the liver and intestine to the central nervous system. Published literature indicates that the sympathetic pathways carry efferent anti-inflammatory signals from the central nervous system to the intestine. The black arrowheads indicate the directions of nerve signaling.

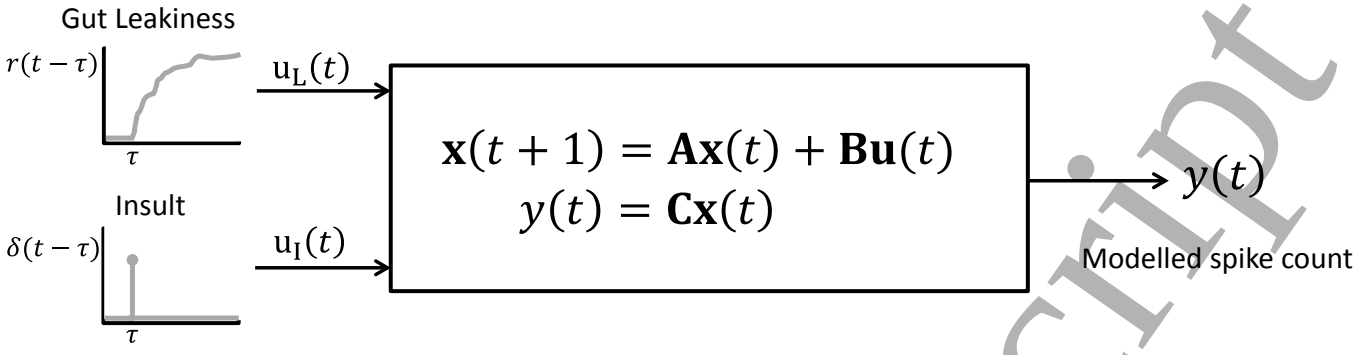

*Figure 2. A schematic of the state-space model. The model has two inputs: an impulse function that represents an insult to the system at time of TNBS injection into the intestinal lumen, at time τ, and a ramp function that represents gut leakiness due to inflammation, measured using impedance data. The output of the system is a time-series of spike counts. The model parameters, **A**, **B**, **C** are optimized such that the modelled spike count time course, y, matches the electrophysiological data.*

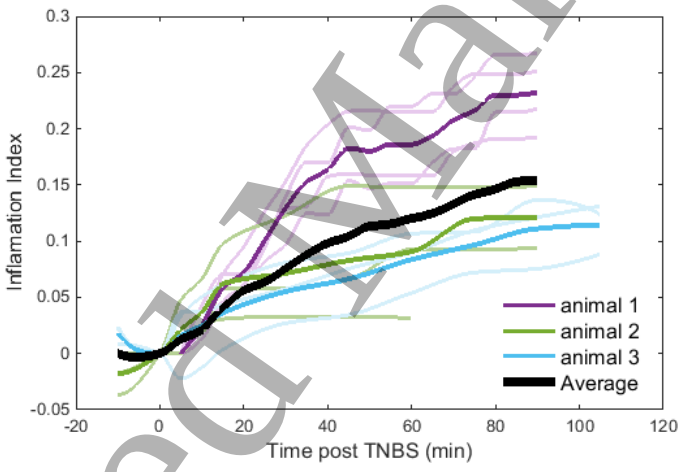

Figure 3. Inflammation index after application of TNBS. A. Inflammation index, r, derived from experimentally recording impedance values in three animals. Each color represents a different animal. Lighter colors: recordings from different electrodes. Darker lines: mean data. Average across animals is shown with the black line. TNBS was nominally applied at time 0.

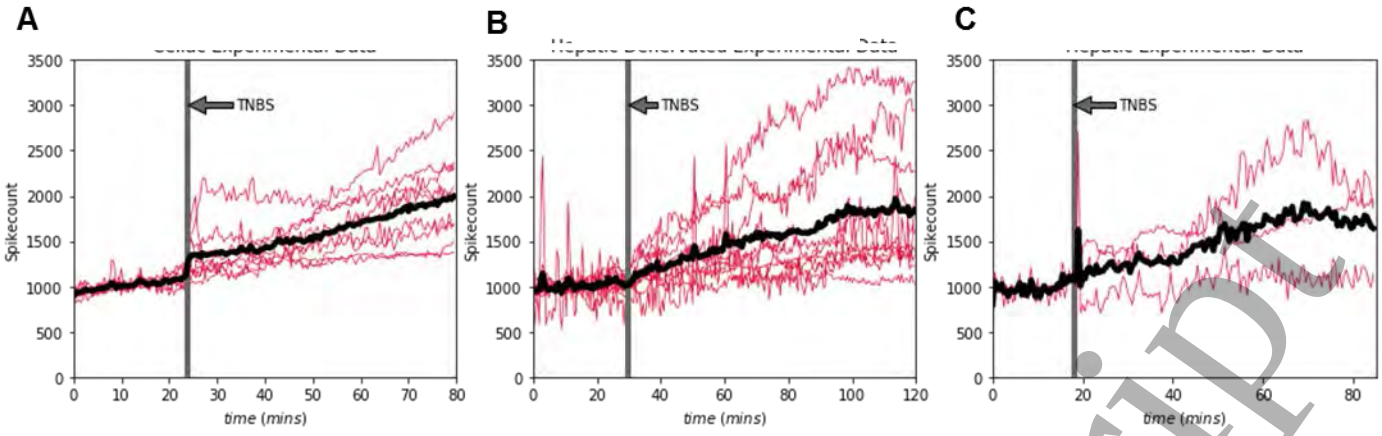

Figure 4. Normalized recordings from vagal afferent pathways. The red lines show data from individual animal experiments and the thick blacks lines are the means across experiments. Spike counts represent the number of spikes in the recorded nerve activity during a 30 second epoch. Spike count data are normalized across experiments such that the activity immediately prior to TNBS is scaled to 1000 counts per 30s epoch. Time of application of TNBS is indicated by the vertical bar. (A) Recordings from the celiac branch of the vagus nerve in 9 rats. (B) Recordings from the hepatic branch of the vagus nerve in 10 rats, where the afferents that originate in the inflamed region had been cut (denervated intestine). (C) Recordings from the hepatic branch of the vagus nerve in 3 rats where the afferents that originate in the inflamed region were not cut (non-denervated intestine).

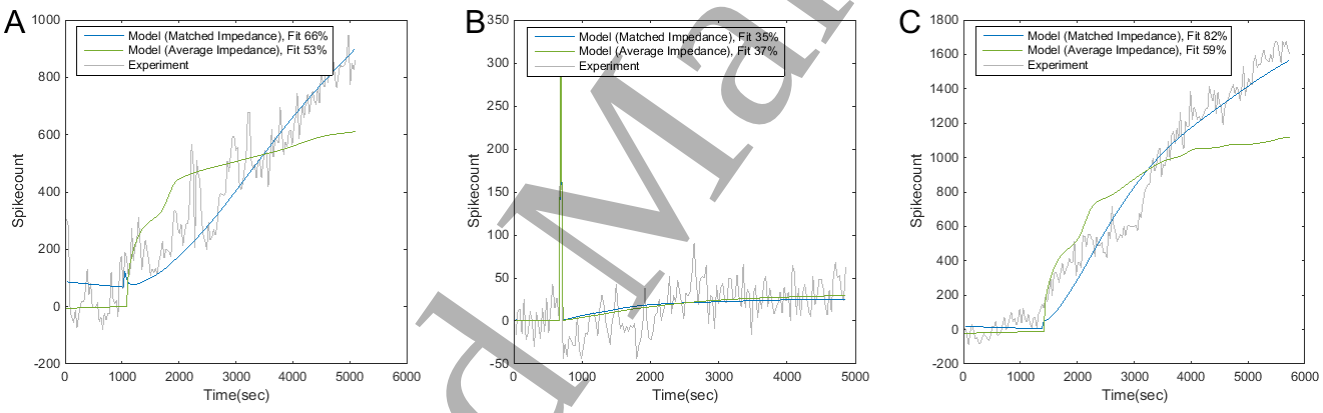

Figure 5. Comparing the state-space model with simultaneously recorded, matched, input impedance (blue) to the model driven by average input impedance (green) across experiments. A. Celiac nerve recording. B, C. Hepatic nerve recordings. Percentage fit calculated using Eq. (3) is shown in the legend. Individual matching is superior to matching against averages.

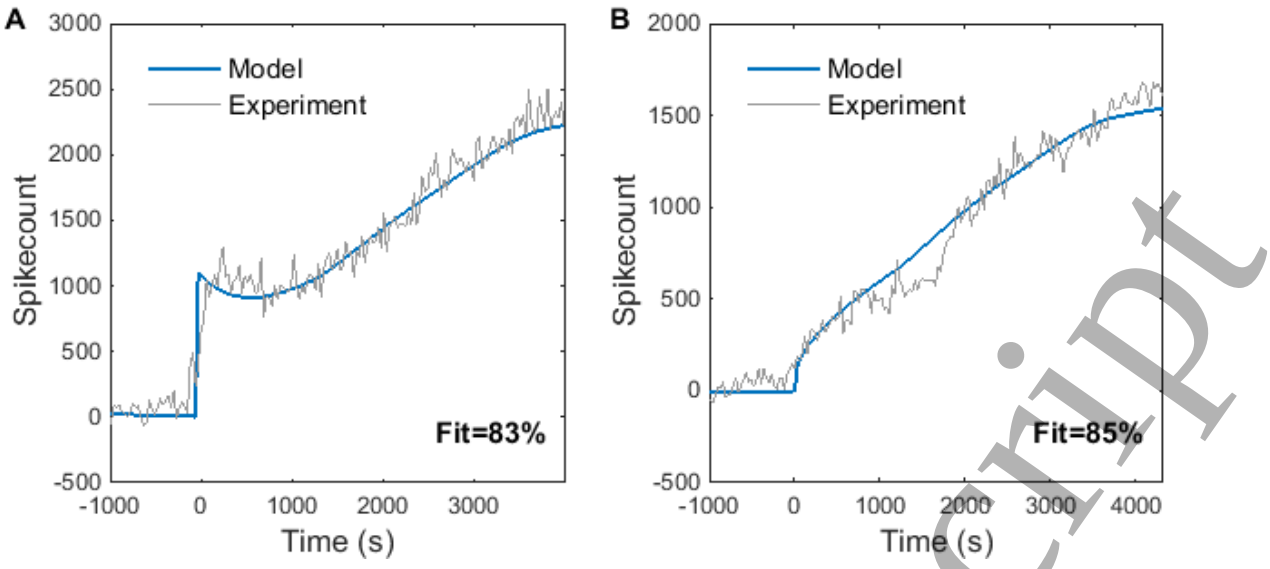

Figure 6. Comparisons of electrophysiological data and state-space model outputs for two examples: A. Celiac nerve and B. Hepatic nerve. The grey lines show recorded spike counts and the blue lines the fitted models. TNBS was applied to the gut at a time zero.

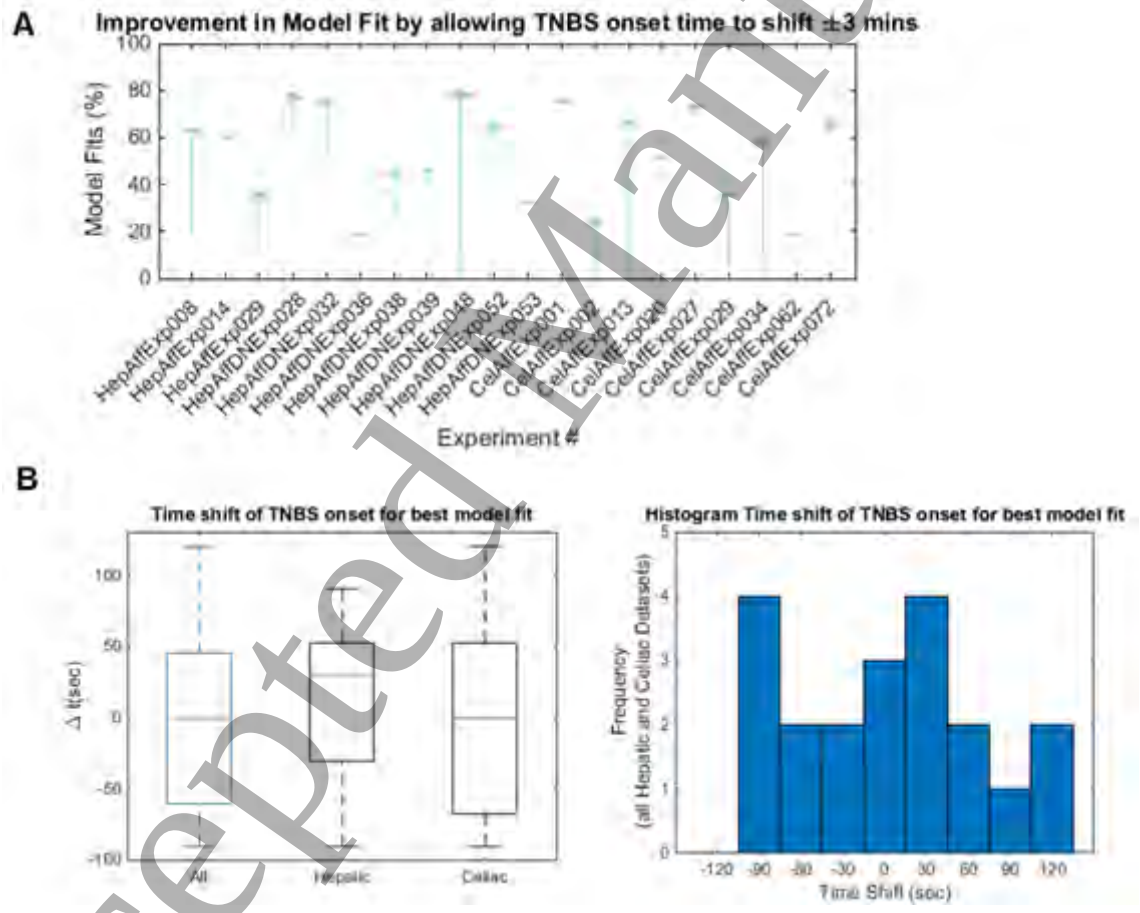

Figure 7. The result of TNBS onset time adjustment. A. Improvement in model fit by allowing adjustment in TNBS onset time. Green arrows show the gains in NRMSE (Normalized Root Mean Squared Error) model fit from the experiment labels of TNBS onset time (at bottom of arrow) to the optimized TNBS onset time (at top of arrow). B. Statistics of TNBS onset shift for best model fit. Left: Time shift of TNBS onset for best model fit. Right: Histogram time shift of TNBS onset for best model fit. Optimized fits required time adjustments of up to – 90 sec and + 120 sec.

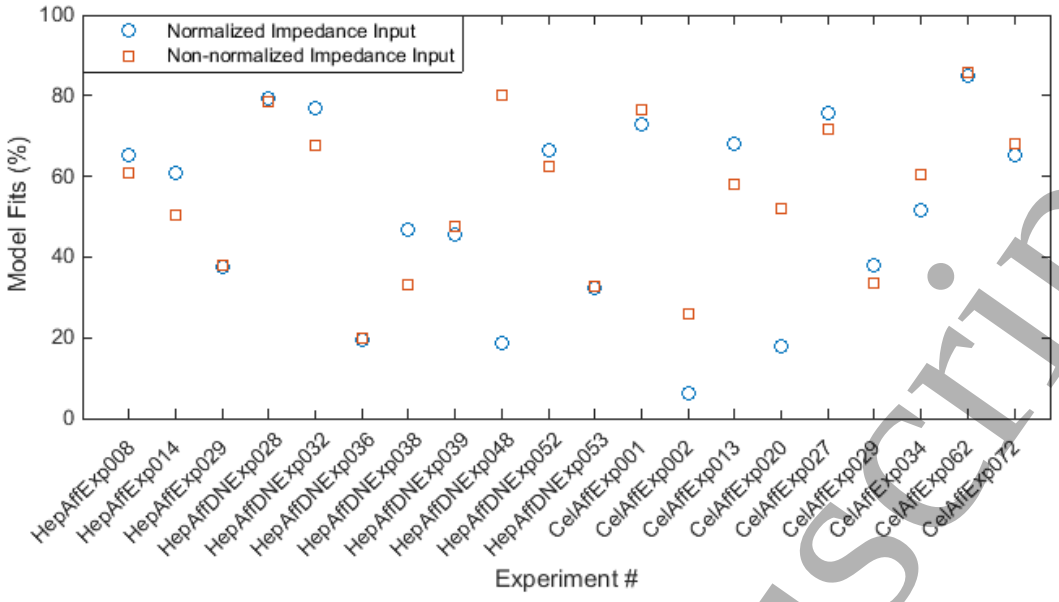

Figure 8. Best model fit with normalized input impedances (circles) vs. non-normalized impedances (squares) across experiments.

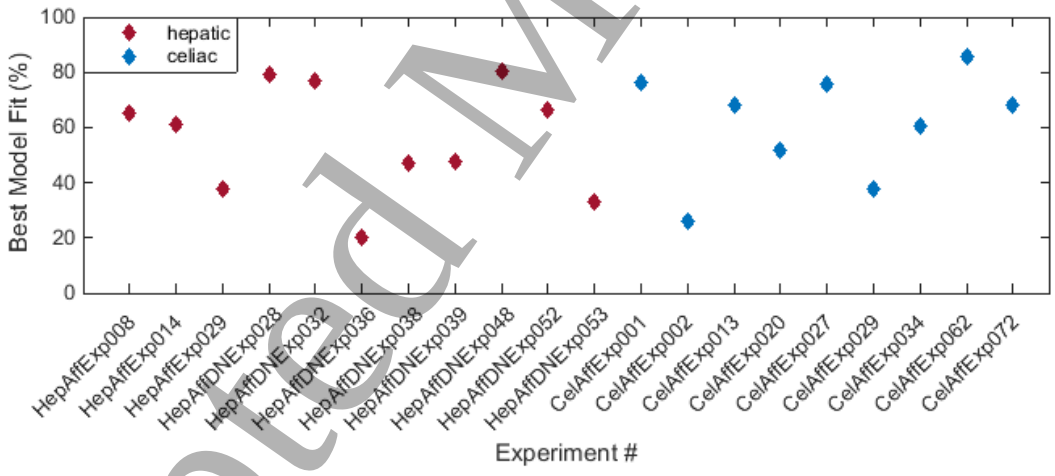

Figure 9. Model fit for different experiments. "Best Model Fit" indicates the NRMSE for the model that has been optimally fit to the data, including adjustment of TNBS onset time.

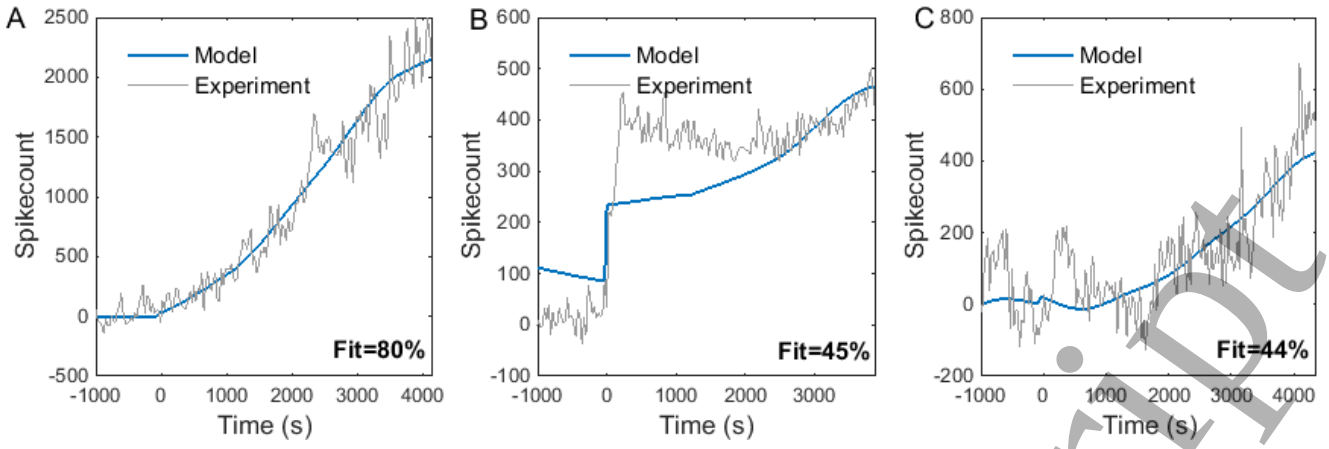

Figure 10. Sample Model Fits. A. An excellent model fit of 80%. B. An ineffective fit of 45%. C. A good fit to the data, but the model fit metric is only 44% due to the high variance of the spike count time series. Experiment spike count variance: A. 0.39 spikes/second; B. 0.27 spikes/second; C. 1 spikes/second.

References

Abbas JJ and Chizeck HJ (1991) Feedback control of coronal plane hip angle in paraplegic subjects using functional neuromuscular stimulation, IEEE Trans Biomed Eng, 38, 687–698.

Berthoud H-R, Carlson NR, Powley TL (1991) Topography of efferent vagal innervations of the rat gastrointestinal tract, Am J Physiol, 260: R200–R207.

Bonaz B, Picq C, Sinneger V, Mayol JF, Clarencon D (2013) Vagus nerve stimulation: from epilepsy to the cholinergic anti-inflammatory pathway, Neurogastroenterol Motil, 25: 208–221.

Bonaz B, Sinniger V, Pellissier S (2016) Anti-inflammatory properties of the vagus nerve: potential therapeutic implications of vagus nerve stimulation, J Physiol,1–10.

Bonaz B, Sinneger V, Hoffmann D, Clarencon D, et al. (2016) Chronic vagus nerve stimulation in Crohn's disease: a 6-month follow-up pilot study, Neurogastroenterol Motif, 28:948–953.

Borovikova LV, Ivanova S, Zhang M, Yang H, et al. (2000) Vagus nerve stimulation attenuates the systemic inflammatory response to endotoxin, Letters to Nature, 405: 458–462.

Bornstein JC,. Furness JB, Kelly HF, Bywater RAR, Neild TO, Bertrand PP (1997) Computer simulation of the enteric neural circuits mediating an ascending reflex: Roles of fast and slow excitatory outputs of sensory neurons, J Autonomic Nerv Sys 64: 143–157.

Chambers JD, Thomas EA, Bornstein JC (2014) Mathematical modelling of enteric neural motor patterns, Clin & Exp Pharma & Physiol, 41: 155–164.

Du P, Poh YC, Lim JL, Gaendiran V, O'Grady G, Buist ML, Pullan AJ, Cheng LK (2011) A preliminary model of gastrointestinal electromechanical coupling, IEEE Trans Biomed Eng, 58(12) : 3491–3495.

Furness JB, Callaghan BP, Rivela LR, Cho HJ (2014) The enteric nervous system and gastrointestinal innervation: integrated local and central control, Adv Exp Med Biol, 817: 39–71.

Furness JB, Johnson PJ, Pompolo S, Bornstein JC (1995) Evidence that enteric motility reflexes can be initiated through entirely intrinsic mechanisms in the guinea-pig small intestine, Neurogastroenterol Motil,7: 89–96

Fountas KN, Smith JR, Murro AM, Politsky J, Park YD, Jenkins PD (2005) Implantation of a closed-loop stimulation in the management of medically refractory focal epilepsy, Stereotact Funct Neuros, 83: 153–158.

Gorzelic P, Schiff SJ, Sinha A (2013) Model-based rational feedback controller design for closed-loop deep brain stimulation of Parkinson's disease, J Neural Eng, 10: 026016.

Gerova VA, Stoynov SG, Katsarov DS, Svinarov DA (2011) Increased intestinal permeability in inflammatory bowel diseases assessed by iohexol test, World J Gastroenterol, 17(17): 2211–2215.

Guiraud D, Andreu D, Bonnet S, Carrault G et al. (2016) Vagus nerve stimulation: state of the art of stimulation and recording strategies to address autonomic function neuromodulation, J Neural Eng 13: 041002.

Hillsley K, Kirkup AJ, Grundy D (1998) Direct and indirect actions of 5-hydroxytryptamine on the discharge of mesenteric afferent fibres innervating the rat jejunum, J Physiol, 506: 551–561.

Horn CC, Friedman MI (2004) Separation of hepatic and gastrointestinal signals from the common “hepatic” branch of the vagus, Am J Physiol, 287: R120–R126.

Ivorra A, Rubinsky B (2007) In vivo electrical impedance measurements during and after electroporation of rat liver, Bioelectrochem, 70(2): 287–295.

Levine YA, Koopman FA, Faltys M, Caravaca A, Bendele A, Zitnik R, Vervoordeldonk MJ, Peter Tak P (2014) Neurostimulation of the cholinergic anti-Inflammatory pathway ameliorates disease in rat collagen-induced arthritis, PLOS One, 9(8), e104530.

Lomax AE, Sharkey KA, Furness JB (2010) The participation of the sympathetic innervation of the gastrointestinal tract in disease states, Neurogastroenterol Motil, 22: 4–18.

Martelli D, McKinley MJ, McAllen RM (2014) The cholinergic anti-inflammatory pathway: a critical review, Auton Neurosci,182: 65–69.

Martelli D, Yao S, McKinley MJ, McAllen RM (2014) Reflex control of inflammation by sympathetic nerves, not the vagus, J Physiol. 2014 Apr 1; 592: 1677-1686.

Munk OL, Keiding S, Bass L (2003) Impulse-response function of splanchnic circulation with model-independent constraints: theory and experimental validation, Am J Physiol Gastrointest Liver Physiol 285: G671–G680.

Nelson TS, Suhr CL, Freestone DR, Lai A, Halliday AJ, McLean KJ, Burkitt AN, Cook MJ (2011) Closed-loop seizure control with very high frequency electrical stimulation at seizure onset in the GEARS model of absence epilepsy, J Neural Sys, 21(2): 163–173.

Niijima A (1996) The afferent discharges from sensors for interleukin 1b in the hepatoportal system in the anesthetized rat, J Auton Nerv Syst, 61: 287–291.

Nicander I, Lundh Rozell B, Rundquist L, Ollmar S (1997) Electrical impedance. A method to evaluate subtle changes of the human oral mucosa, Europ J of Oral Sci, 6: 576–582.

Pappenheimer JR, Volpp K (1992) Transmucosal impedance of small intestine: correlation with transport of sugars and amino acids, Am J Physiol, 263(2 Pt 1): C480–493.

Pavlov VA, Tracey KJ (2005) The cholinergic anti-inflammatory pathway. Brain Behav Immun,19(6): 493–499.

Payne SC, Shepherd RK, Sedo A, Fallon JB, Furness JB (2018) Anobjective in vivo diagnostic method for inflammatory bowel disease. Royal Society Open Science, 5: 180107.

Phillips RJ, Baronowsky EA, Powley TL (1997) Afferent innervation of gastrointestinal tract smooth muscle by the hepatic branch of the vagus, J Comp Neurol, 384: 248–270.

Prechtl JC, Powley TL (1987) A light and electron microscopic examination of the vagal hepatic branch of the rat, Anat Embryol, 176:115–126.

Rosin B, Slovik M, Mitelman R, Rivlin-Etzion M, Haber SN, Israel Z, Vaadia E, Bergman H (2011) Closed-loop deep brain stimulation is superior in ameliorating Parkinsonism, Neuron, 72(2): 370–384.

Stakenborg N, Famm K, Litt B, Slaouli M (2013) Drug discovery: a jump-start for electroceuticals, Nature: 159–161.

Stakenborg N, Wolthuis AM, Gomez-Pinilla PJ, Farro G, Di Giovangiulio M, Bosmmans G, Labeeuw E et al. (2017) Abdominal vagus nerve stimulation as a new therapeutic approach to prevent postoperative ileus, Neurogastroenterol Motil, e13075.

Stemberg EM (1997) Neural-immune interactions in health and disease, J Clin Invest, 100(11): 264 –2647.

Tukhlina N and Rosenblum M (2008) Feedback suppression of neural synchrony in two interacting populations by vanishing stimulation, J Biol Physics, 34: 301–314.

Yamakawa K, Matsumoto N, Imamura Y, Muroya T et al (2013) Electrical vagus nerve stimulation attenuates systemic inflammation and improves survival in a rat heatstroke model, PLOS One, 8(2), e56728.

Zimmermann JB and Jackson A (2014) Closed-loop control of spinal cord stimulation to restore hand function after paralysis, Frontiers in Neurosci, 10, 33–89.

Willemze RA, Luyer MD, Buurman WA, de Jonge WJ (2015) A neural reflex pathways in intestinal inflammation: hypotheses to viable therapy, Nat Rev Gastroenterol Hepatol, 12: 353–362.

Willemze RA, Welting O, van Hamersveld HP, Meijer SL, Folgering JHA, Darwinkel H, Witherington J, Sridhar A, Vervoordeldonk NJ, Seppen J, de Jonge WJ (2017) Neuronal control of experimental colitis occurs via sympathetic intestinal innervation, Neurogastrien & Motility, e13163.